Through-space conjugation-dominated luminescence mechanism

Bo Wu[1,2], Guoqing Zhang[2], Zheng Zhao[1]* and Ben Zhong Tang[1]*

[1]School of Science and Engineering, Shenzhen Institute of Aggregate Science and Technology, The Chinese University of Hong Kong, Shenzhen (CUHK-Shenzhen), Guangdong 518172, China.

[2]Hefei National Research Center for Physical Sciences at the Microscale, University of Science and Technology of China, Hefei, 230026 China

*Corresponding author:

E-mail address:

zhaozheng@cuhk.edu.cn (Z. Zhao)

tangbenz@cuhk.edu.cn (B.Z. Thang)

TOC

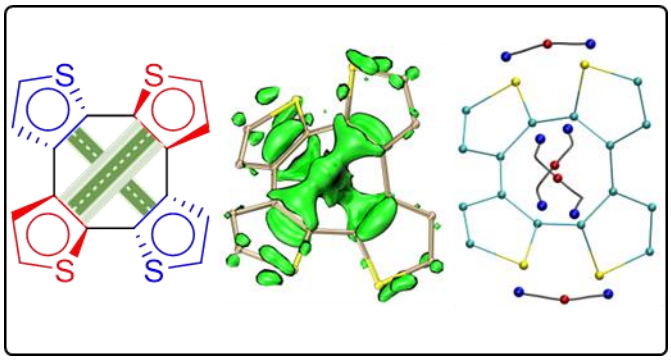

This work discovered the ‘conjugation anomalous' luminescence behavior of COTh and systematically proved its unique TSC-dominated luminescence mechanism. COTh exhibited a particular overpass-shaped TSC channel that cut through the molecule and effectively linked the four thiophene rings. Furthermore, a TSC analysis tool was developed to obtain accurate TSC paths and intensities.

Abstract

The influence of through-space conjugation (TSC) on the optical properties of molecules was consistently neglected in past research. Recently, TSC-related luminescence phenomena were reported sporadically, but a general lack of in-depth understanding of the TSC luminescence mechanism exists. The TSC factors, TSC intensity, and the impact of TSC on material properties remained theoretical blind spots. This work selected cyclooctatetrathiophene (COTh) as a research model and comprehensively analyzed the nature of TSC at the experimental and theoretical levels. The COTh molecule exhibited an anomalous luminescence that did not match the degree of through-bond conjugation. Instead, it was determined to be a luminescence phenomenon dominated by TSC. A unique overpass-shaped TSC channel was the key to achieving TSC-dominated luminescence. Orbital phase, angle, and spatial distance were essential factors in forming an effective TSC channel. Moreover, both COTh isomers and aryl-substituted COTh derivatives were shown to possess TSC-dominated luminescence properties, which provided sufficient evidence for the TSC-dominated luminescence mechanism. In addition, a practical TSC analysis tool was developed that could quickly analyze the TSC path, action location, and action intensity for any molecular system. This work will provide helpful guidance and inspiration for TSC research and promote the development of TSC-related research.

Keywords:

Through-Space Conjugation, Cyclooctatetrathiophene, Luminescent Properties, Aggregation-Induced Emission, Non-Bonded Interactions

Introduction

In classical organic photophysics, the through-bond conjugation (TBC) is considered necessary for efficient visible light emission.[1, 2] The degree of TBC significantly affects organic molecules' fluorescence efficiency and emission color. By adjusting the TBC, materials with various luminescent colors from ultraviolet to near-infrared wavelengths were obtained,[3, 4] widely used in fields such as fabric dyes, optoelectronic displays, and biomarkers.[5-7] With the development of organic photophysics, TBC concepts have continuously innovated and improved. For example, the concept of twisted intramolecular charge transfer clarifies the solvent polarity-dependent characteristics of the donor-acceptor system and the nature of the charge transfer and local excitation.[8, 9] The concepts of photoinduced electron transfer and excited-state intramolecular proton transfer reveal the electron and proton transfer process in the excited state.[10, 11] Circularly polarized luminescence emphasizes the synergistic effect of the chiral center of the molecule and the TBC.[12-14] These emerging concepts about TBC promoted the wide application of optical materials.

With the deepening of research, it is gradually realized that non-bonded interactions play an essential role in molecular structure and optical properties.[15, 16] For planar molecules, there are many important concepts of nonbonded interactions. For example, pi-pi interactions often lead to planar packing patterns in crystals.[17, 18] Excimers and ground-state donor-acceptor complexes describe the effect of dimers on the ground- and excited-state optical properties of the molecule.[19-21] J- and H- aggregates emphasize the influence of different alignment orientations on molecular energy levels and transition dipole moments.[22, 23] Non-planar and flexible molecules often exhibit diverse optical properties in solution and crystal, fundamentally caused by different non-bonded interactions within or between molecules. The aggregation-induced emission (AIE) proposal is an important breakthrough in researching non-bonded interactions.[24-29] The optical properties of AIEgen with rotor structures are sensitive to the twist angle of rotor. For rotor-less AIEgen, their luminescence properties are sensitive to the flexible vibration of molecular skeletons. Strong non-bonded interactions could restrict intramolecular rotation or vibration, significantly weakening excitons' non-radiative dissipation and improving optical properties.[30-32] Theories related to non-bonded interactions have given rise to many new

organic optical materials with excellent application prospects.

Through-space conjugation (TSC) is an emerging concept related to non-bonded interactions.[33] Spatial overlap of orbitals and electrons between non-adjacent groups is common in most molecules, especially in non-planar molecules.[34, 35] The through-space interactions have essential effects on molecules' overall conjugation degree but have been ignored in past studies. Until recently, sporadic literature reported TSC-related luminescence[36-38] but was limited to a surface-level description of luminescence behavior and lacked an in-depth analysis of the TSC mechanism. So far, the TSC formation factors, TSC strength, and influence of TSC on material properties are still theoretical blind spots, which seriously restricts the development of TSC theory.

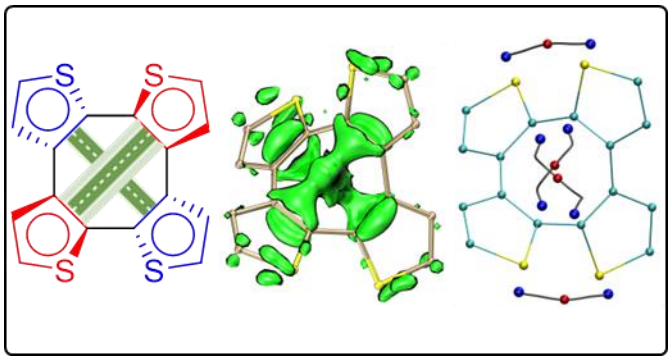

Scheme 1. A new TSC type in COTh: an overpass-shaped TSC channel cut through the molecule and effectively links the four thiophene rings.

This work discovered a class of model molecules suitable for studying TSC: cyclooctatetrathiophene (COTh), which showed TSC-dominated rather than TBC-dominated luminescence properties. The TSC-dominated luminescence mechanism was comprehensively revealed. As shown in **Scheme 1,** COTh molecules exhibit a new TSC type: an overpass-shaped channel cut through the molecule and effectively links the four thiophene rings. It significantly increases the overall conjugation degree of the system. Orbital phase, angle, and spatial action distance were critical factors in the formation of TSC. Furthermore, COTh isomers and aryl-substituted COTh derivatives were also established to possess TSC-dominated luminescence characteristics. To scan different TSC pathways and compare TSC intensities, an efficient TSC analysis tool was developed,

which would provide convenience for TSC-related research.

Main text

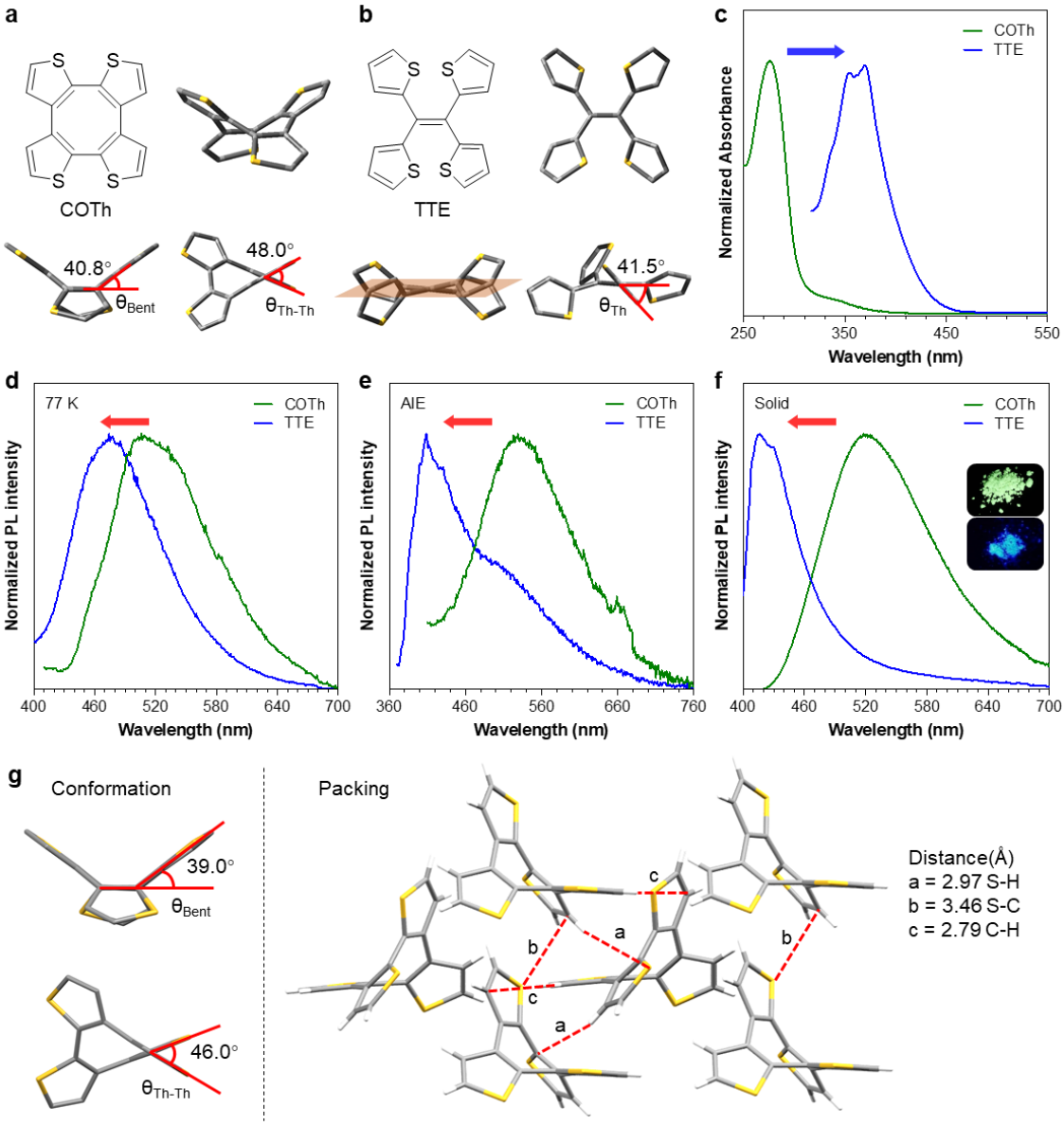

Figure 1.
(a-b) Chemical structures and theoretical optimized structure of (a) COTh and (b) TTE.
(c) Normalized absorption spectra of COTh and TTE in THF solution.
(d-f) Normalized PL spectra of COTh and TTE (d) in 2-MeTHF at 77 K, (e) in acetone/water mixtures at 90% water fractions, and (f) at solid states. [COTh] = [TTE] = 10^{-5} M, λ_{ex} (TTE) = 320 nm, λ_{ex} (COTh) = 350 nm.
(g) Conformations and molecular packing arrangements in the crystals of COTh.

COTh and tetrathienylethene (TTE) are two AIE molecules of the tetrathiophene system recently reported by our group.[39, 40] Their compositions are similar, but their

luminescent properties differ. The chemical structures and theoretically optimized structure of COTh and TTE are shown in Figures 1a and 1b. The TBC units of COTh include four thiophenes and an 8-membered ring structure, and the TBC units of TTE include four thiophenes and a double bond. The theoretical optimization results show that COTh exhibits a saddle-shaped structure with no obvious molecular plane. The average bent angle (θ_{Bent}) of its cyclooctatetraene (COT) core is 40.8°, and the average dihedral angle ($\theta_{Th\text{-}Th}$) between adjacent thiophenes is 48.0°, indicating that the degree of conjugation between thiophenes may be poor. The structure of TTE has a central plane centered on the double bond, which means that the four thiophene rings can be effectively conjugated through this central plane. It is well known that the 2-position of thiophene has greater conjugation activity than the 3-position, so the substitution position of the thiophene ring also affects the TBC degree of COTh and TTE. For COTh, the connection types between thiophene rings include two 2-, 2-position connections and two 3-, 3-position connections. The 3-, 3-position connection will reduce the TBC degree of COTh. The four thiophenes of TTE are all connected to double bonds through the 2-position, which allows all thiophenes to participate in TBC effectively. Judging from the molecular structure, the TBC degree of COTh is smaller than that of TTE.

The UV absorption spectra of COTh and TTE (Figure 1c) confirmed their TBC degree. The longest wavelength absorption peak and onset of COTh were located at 340 nm (a shoulder peak) and 400 nm, while the longest wavelength absorption peak and onset of TTE were located at 365 nm and 413 nm, which verified that the TBC degree of COTh was indeed worse than that of TTE. Then, the photoluminescence (PL) properties of COTh and TTE in various states were studied. No luminescence was detected in solution at room temperature for either molecule, which was attributed to their strong quenching pathways in the free state. PL spectra of COTh and TTE in 2-MeTHF at 77 K (Figure 1d) showed that the emission peak of TTE was located at 475 nm while the emission peak of COTh was located at 508 nm. Compared to TTE, COTh had worse conjugation but emitted at a longer wavelength at low temperatures, which was a special ‘conjugation anomalous’ luminescence behavior. The emission spectra of COTh and TTE in the aggregated state (Figures 1e and S1) and crystal state (Figure 1f) were recorded to explore this abnormal luminescence behavior further. The emission wavelengths of COTh and TTE were 410 nm

and 530 nm, respectively, in the aggregate state and 520 nm and 415 nm in the crystal state, indicating that COTh exhibited 'conjugation anomalous' luminescence behavior in various states.

Large changes in emission wavelength are usually attributed to large changes in molecular structure or strong intermolecular pi-pi stacking. However, these explanations do not apply to the abnormal luminescence behavior of COTh. On the one hand, in the 77 K frozen state, aggregates state, and crystal state, the huge steric hindrance made large structural changes impossible. On the other hand, the emission wavelengths of COTh in the single molecule state (77 K) and the stacked state (aggregated state and crystal state) were similar, indicating that the intermolecular interaction of COTh had little impact on its conjugation degree and luminescent property. More information on intermolecular interactions can be obtained by analyzing crystal structures. Conformations and molecular packing arrangements in the crystals of COTh and TTE are shown in Figures 1g and S2. COTh crystal structure exhibited a saddle shape similar to that of the optimized monomer structure, with only slight changes in bent angle θ_{Bent} and dihedral angle $\theta_{Th\text{-}Th}$, which made it difficult to form effective parallel stacking. Abundant weak intermolecular interactions such as S···H, C···H, and S···C were observed, which could restrict intramolecular motions and enhance the luminescence of COTh. However, no pi-pi stacking was observed, which further suggested that the 'conjugate anomalous' luminescence of COTh was an intramolecular rather than intermolecular behavior.

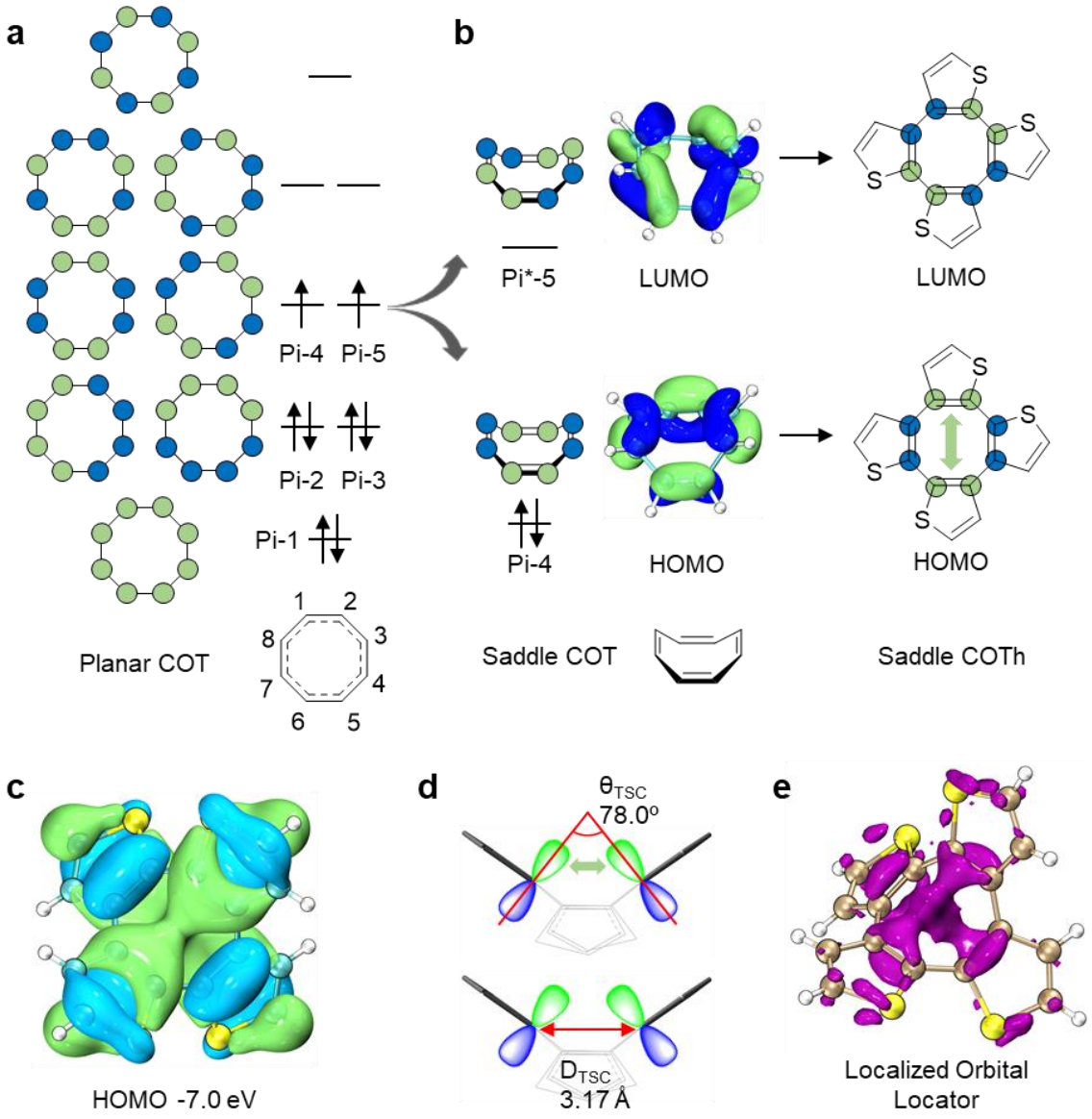

Figure 2.
(a) Orbital diagrams of theoretically planar COT.
(b) Orbital diagrams of saddle-shaped COT and COTh.
(c) Electron density distribution of HOMO of COTh.
(d) TSC angles θ_{TSC} and distances D_{TSC} of saddle-shaped COTh.
(e) LOL analysis of HOMO of COTh. Isosurface = 0.2.

COTh is an anti-aromatic molecule due to its 8-membered ring structure, and its properties differ significantly from ordinary aromatic organic molecules.[41] Therefore, we speculate that its abnormal luminescence may be related to the 8-membered ring structure of its COT core. According to the molecular orbital theory, the phase and energy level of

the pi orbital of the planar COT ring with D8h symmetry are shown in Figure 2a. The two high-energy occupied orbitals pi-4 and pi-5 are the degenerate singly occupied molecular orbital (SOMO) orbitals, and their high energy comes from the special phase arrangement of eight conjugated p orbitals.[42, 43] When p orbitals in the same phase are combined, the energy of the orbitals will decrease. In contrast, when p orbitals in opposite phases are combined, the energy of the orbitals will increase. For pi-4 orbit, there are four positions with the same phase and four positions with opposite phases, which results in the energy of the pi-4 orbital being as high as the energy of the atomic orbital before the combination. The same goes for the pi-5 orbital. These two high-energy orbitals prevent the stable existence of a planar COT ring with D8h symmetry, so the molecule bends from the plane to a saddle shape in the actual stable COT configuration. With the change of configuration, the original two high-energy degenerate orbitals pi-4 and pi-5 in planar COT become the highest occupied molecular orbital (HOMO) and lowest unoccupied molecular orbital (LUMO) in saddle-shaped COT, respectively (Figure 2b). However, their phase arrangement remains unchanged, meaning these orbitals are less delocalized.[44] When the system is extended from COT to COTh, HOMO still exhibits this phase arrangement which is not conducive to through-bond delocalization, which means that it is difficult for electrons of HOMO to delocalize to the region between adjacent thiophenes.

Theoretical transition analysis showed that radiative transition of COTh was dominated by HOMO and LUMO (Table S1). The HOMO and LUMO electron density distribution are shown in Figures 2c and S3. To conveniently describe different thiophene positions, the adjacent thiophene rings are defined as ortho-thiophenes, and the non-adjacent thiophene rings are defined as para-thiophenes (Figure S4). The opposite phases between ortho-thiophenes hindered the through-bond delocalization between them. However, the phases between para-thiophenes were the same, which meant the TSC effect between them was possible if their distance was close enough. Figure 2c shows that COTh exhibited distinct through-space electronic delocalization channels originating from para-thiophenes. As shown in Figures 2d and S5, two structural parameters were used to characterize the TSC interaction between para-thiophenes: (1) θ_{TSC}, the angle between the p orbitals of two para-thiophene; (2) D_{TSC}, the average distance between the double bonds of two para-thiophene. The larger θ_{TSC} or the smaller D_{TSC}, the greater the TSC interaction

between the two para-thiophene. In the crystal structure of COTh, the D_{TSC} was 3.17 Å, much shorter than the sum of the van der Waals radii of two C atoms (3.40 Å). Therefore, there was adequate through-space orbital overlap between the para-position double bonds. Localized orbital locator (LOL) analysis was performed to analyze the correlation between the delocalization characteristics of molecular orbitals and traditional chemical bonds (Figure 2e). The functions of LOL analysis are explained and shown in Figure S6. The results of LOL analysis showed that the HOMO did not correspond to any double bond but corresponded to a through-space channel, proving that electrons in HOMO tended to remain in the TSC region. Even more surprising is that the upper and lower TSC channels were connected through a channel that penetrated the COT ring, forming an overpass-shaped TSC channel and significantly increasing the molecules' overall conjugation degree. This novel TSC channel completely subverts the traditional concept of delocalization paths and expands the dimensions and forms of non-traditional delocalization. The impact of the TSC channel on photophysical properties, such as electron distribution and transition processes, was further analyzed. The results of HOMO electron distribution analysis based on the NAO method are shown in Figure S7 and Table S2. The total contribution of the COT core (C1-C8) was up to 67%, indicating that the overpass-shaped TSC channel made HOMO orbital electrons tend to concentrate in the COT core region. The electron density difference before (lowest excited singlet state, S_1) and after (ground state, S_0) the radiative transition is shown in Figure S8. The electron density in the TSC channel changed significantly, which proved that the TSC channel was very involved in the transition process.

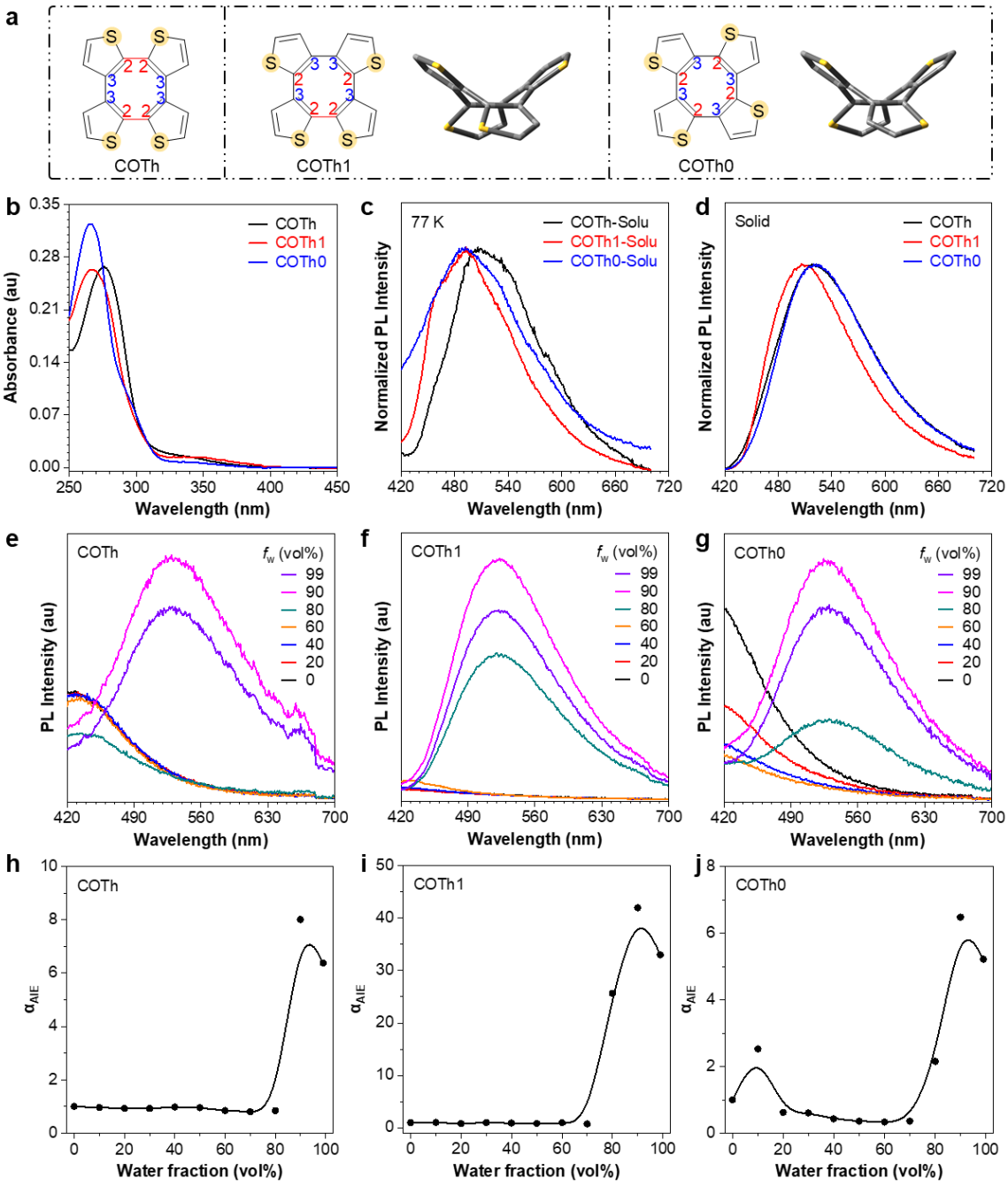

Figure 3.

(a) Chemical structures and theoretical optimized structures of isomers: COTh, COTh1, and COTh0.

(b) Absorption spectra of COTh, COTh1, and COTh0 in THF solution.

(c-d) Normalized PL spectra of COTh, COTh1, and COTh0 (c) in 2-MeTHF at 77 K and (d) at solid states.

(e-g) PL spectra of (e) COTh, (f) COTh1, and (g) COTh0 in THF/water mixtures with different water fractions.

(h-j) Plots of relative PL intensity (α_{AIE}) of (h) COTh, (i) COTh1, and (j) COTh0 versus

water fraction in acetone/water mixtures. [COTh] = [COTh1] = [COTh0] = 10^{-5} M, λ_{ex} = 350 nm.

As reported in our previous work,[40] S-S interaction between adjacent thiophene rings may also affect molecular properties. To compare the impact of overpass-shaped TSC and S-S interaction, three COTh isomers with different thiophene ring arrangements were designed. As shown in Figure S9, the different arrangements of the thiophene rings resulted in different potential S-S interaction paths in the isomers: 2 paths for COTh, 1 for COTh1, and 0 for COTh0. Both COTh1 and COTh0 molecules exhibited a saddle-shaped structure similar to the COTh molecule. Figure 3b shows the absorption spectra of COTh, COTh1, and COTh0, from which can be seen that the three COTh isomers all exhibited a weak absorption peak around 340 nm and a strong absorption peak around 265 nm, indicating that their TBC degrees were similar. PL spectra of isomers in 2-MeTHF at 77 K and in crystal state are shown in Figures 3c and 3d. The emission wavelengths of COTh, COTh1, and COTh0 in the 2-MeTHF solution were 510 nm, 490 nm, and 490 nm, respectively. Their minor differences may be attributed to different ways of linking the adjacent thiophene rings. In the crystal state, the emission wavelengths of COTh, COTh1, and COTh0 were 520 nm, 510 nm, and 520 nm, respectively. The slight differences may originate from different intermolecular interactions in the crystal. To further understand the luminescence properties during the aggregation process, the PL spectra of COTh (e), COTh1 (f), and COTh0 (g) in THF/water mixtures with different water fractions (f_W) from 0% to 99% were recorded (Figures 3e-3j). When the water fraction was lower than 80%, none of the three isomers emitted noticeable light. When the fraction was higher than 80%, a broad emission peak around 520 nm appeared in the spectra of all three isomers. When the water content increased from 80% to 99%, the luminescence intensity changed, but the luminescence wavelength did not change, indicating that the enhanced intermolecular interaction during the aggregation process did not affect the molecular configuration for the luminescence process. On the one hand, three isomers all exhibited 'conjugated anomalous' luminescence properties, indicating that the S-S interaction between adjacent thiophene rings did not significantly impact this property. On the other hand, the similar emission wavelengths in monomers, aggregated states, and crystals indicated that the emission transition processes of all three isomers were dominated by intramolecular rather

than intermolecular interactions.

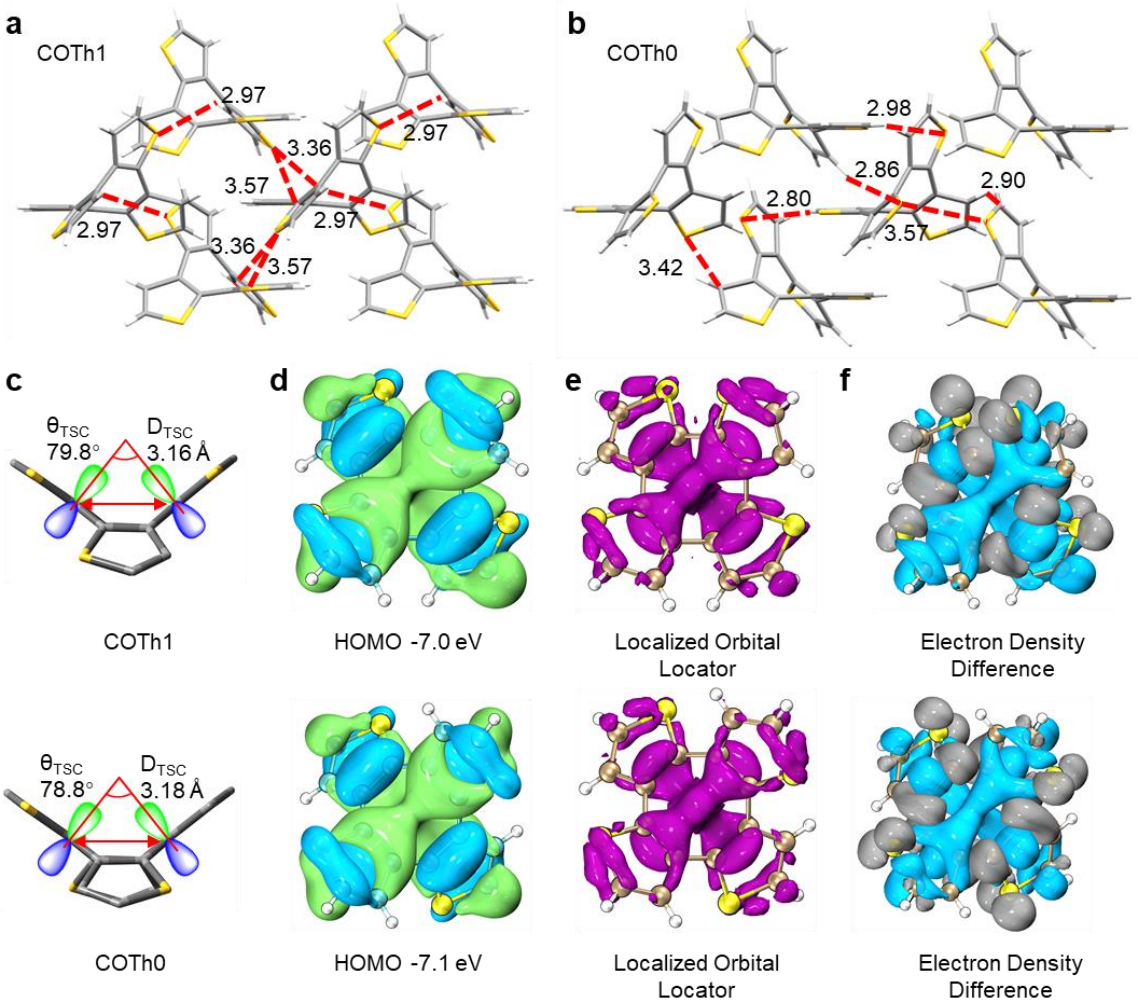

Figure 4.
(a-b) Molecular packing arrangements and intermolecular interactions in the crystals of (a) COTh1 and (b) COTh0.
(c) Bent angles θ_{Bent} and TSC distances D_{TSC} of COTh1 and COTh0.
(d) Electron density distributions and energies of HOMOs of COTh1 and COTh0.
(e) LOL analysis of HOMOs of COTh1 and COTh0. Isosurface = 0.2
(f) Electron density difference between S_1 and S_0 states of COTh. (Density increase, gray; density decrease, blue).

Figures 4a and 4b show the crystal structure of COTh1 and COTh0. Their non-planar saddle shapes were similar to the crystal configuration of COTh. Abundant weak intermolecular interactions such as S···H and C···H were observed, which meant that these intermolecular interactions inhibited the movement of molecules during the aggregation process and led to AIE phenomenon. No intermolecular pi-pi stacking was observed, indicating the 'conjugated anomalous luminescence' of the three isomers is not an

intermolecular behavior.

Comprehensive theoretical analysis was performed to explore the TSC effects on the photophysical properties of COTh1 and COTh0, according to the TSC critical factors discussed in Figure 2, such as orbital phase, interaction distance, and contribution to transition. As shown in Figures 4c and S10, the θ_{TSC} angle between the p orbitals of two para-thiophene in COTh1 and COTh0 were 79.8° and 78.8°, which were almost the same as that of COTh. The average TSC distance D_{TSC} in COTh1 and COTh0 were 3.16 Å and 3.18 Å, respectively, which were much shorter than the sum of the van der Waals radii of two C atoms, indicating there was effective through-space orbital overlap between the para-position double bonds. The HOMOs of COTh1 and COTh0 both show phase arrangements consistent with COTh molecules (Figures 4d and S11). The LOL analysis showed that both COTh1 and COTh0 had novel overpass-shaped TSC channels connecting four thiophenes (Figure 4e). The NAO analysis of HOMO showed that the electrons tended to be distributed in the COT core (Table S3 and Table S4), and the electron density difference analysis (Figure 4f) showed that the electron density in the TSC region changed significantly during the transition process, proving that overpass-shaped TSC channels deeply affected the luminescence property.

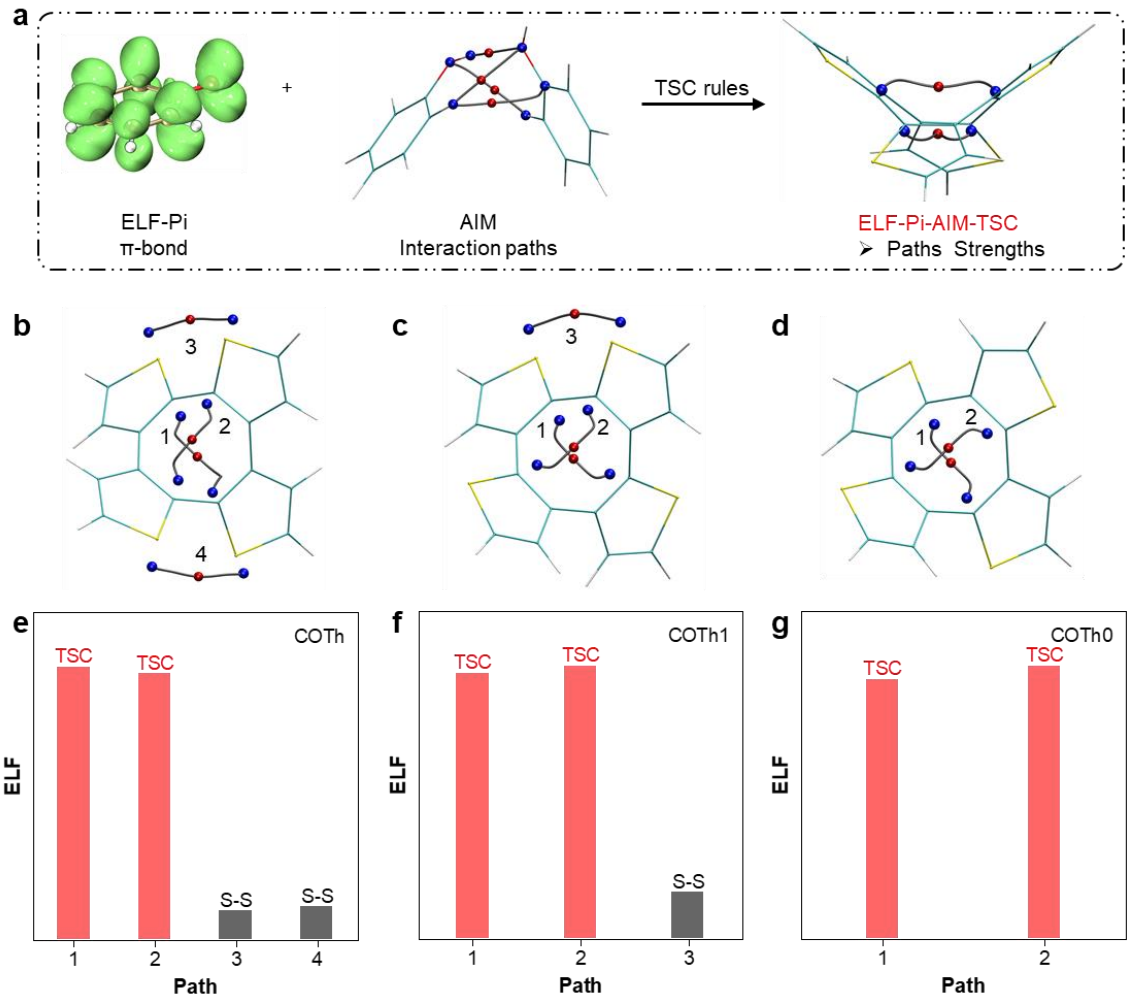

Figure 5.
(a) Schematic diagram of TSC analysis tools ELF-Pi-AIM-TSC.
(b-d) Scanned TSC paths and critical points of (b) COTh, (c) COTh0, and (d) COTh1 through the ELF-Pi-AIM-TSC analysis tool. The blue dots are the starting points of TSC, and the red dots are critical points of TSC.
(e-g) ELF values at critical points on each TSC path of (e) COTh, (f) COTh1, and (g) COTh0.

Although the existence of TSC has been confirmed, some convincing quantitative evidence is still needed to compare the influence of the TSC pathway and potentially other pathways (e.g., S-S interactions) on the optical properties. To solve this problem, we developed a method to quickly find interaction pathways of TSC and quantify the conjugation degrees (Figure 5a). Briefly, by combining the ELF-Pi method used for analyzing the delocalization of pi orbitals and the Atoms-in-Molecules (AIM) method used to explore interaction pathways, many complex orbital interaction pathways could be obtained.[45-47] Further, special rules were formulated based on the through-space property

of the TSC to quickly filter out TSC channels and output the paths, critical points, and TSC intensity. This comprehensive approach was named ELF-Pi-AIM-TSC. The analysis results of COTh, COTh0, and COTh1 using the ELF-Pi-AIM-TSC tool are shown in Figures 5b-5d. The blue dots were the starting points of TSC, and the red dots were critical points of TSC. As expected, S-S interaction paths and overpass-shaped TSC paths were accurately scanned. All three isomers had two overpass-shaped TSC paths connecting the para-position double bonds. The starting point (blue dots) of the TSC paths was all towards the 2-position of thiophene because the conjugation activity of the 2-position is more potent than that of the 3-position. The critical point of interaction (red dots) was located near the center of the COT core. The S-S interaction paths exhibited differences: two S-S paths were scanned in COTh, one S-S path was scanned in COTh1, and no S-S path was observed in COTh0. The ELF value at the critical point in the interaction path represented the degree of delocalization of pi electrons (Figures 5e-5g). The ELF value of TSC paths was much higher than that of S-S paths, proving that the TSC channels played a dominant role in electron delocalization and molecular photophysical properties.

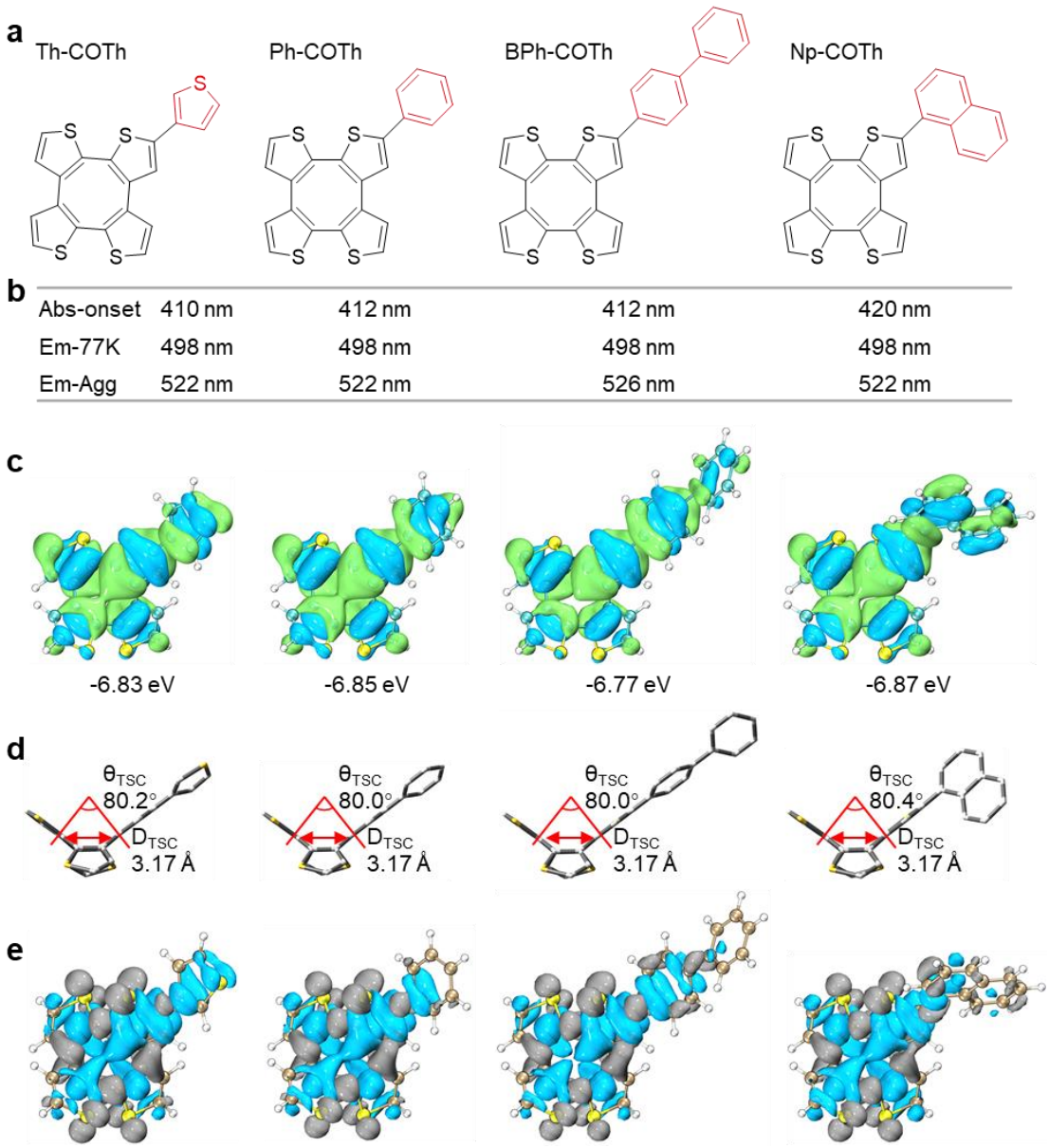

Figure 6.

(a) Chemical structures and abbreviation of aryl substituted COTh derivatives COTh-Ar: Th-COTh, Ph-COTh, BPh-COTh, and Np-COTh.

(b) Absorption onset and emission wavelengths of COTh-Ar derivatives in THF solution at 298 K and in 2-MeTHF at 77 K and at aggregated state.

(c) Electron density distributions and energies of HOMOs of COTh-Ar derivatives.

(d) Bent angles θ_{Bent} and TSC distances D_{TSC} of COTh-Ar derivatives.

(e) Electron density difference between S_1 and S_0 states of COTh. (Density increase, gray; density decrease, blue).

In addition to the thiophene connection mode, aryl substitution (COTh-Ar) may also affect the optical properties of COTh molecules. Therefore, we studied the photophysical properties of several differently aryl-substituted COTh (Figure 6a): thienyl-COTh (Th-COTh), phenyl-COTh (Ph-COTh), biphenyl-COTh (BPh-COTh), naphthyl-COTh (Np-COTh).[48] These different forms of aromatic substituents change the number of conjugated pi electrons in the system and may also change the conjugated electron distribution. The absorption onsets in THF solution and emission wavelengths in 2-MeTHF (77 K) and at the aggregated state of COTh-Ar derivatives are shown in Figure 6b. The similar absorption onsets of these COTh-Ar derivatives indicated their TBC degrees were identical. Their emission wavelengths were around 498 nm in 2-MeTHF at 77 K and 522 nm at the aggregated state. Although COTh-Ar derivatives have different aryl substituents, they all exhibited similar 'conjugate anomalous' luminescence, suggesting that the same factors dominated their emission.

The HOMOs and LUMOs are shown in Figures 6c and S12. The phase arrangements of COT cores in these derivatives were the same as those of COTh. Although the electron distribution range of HOMOs in COTh-Ar derivatives extended to aryl substituent, their HOMO energies only fluctuated within a narrow range from -6.77 eV to -6.87 eV, indicating that the critical factor affecting HOMO energy was the similar COT core rather than the aromatic substituent. The stable structures of COTh-Ar derivatives obtained by theoretical optimization are shown in Figure 6d. The types and twist angles of their aromatic substituents differ significantly (Figure S13), but the TSC angles (θ_{TSC}) and the TSC distances (D_{TSC}) between para-thiophene are almost the same. As with COTh, these TSC angles and TSC distances are highly favorable for the formation of TSC. LOL analysis showed that HOMO electrons in all COTh-Ar derivatives tended to delocalize in the overpass-shaped TSC channels in the COT core (Figure S14). Figure 6e shows the electron density differences before and after the transition in COTh-Ar derivatives. Most electron density changes occurred in the COTh cores, especially in overpass-shaped TSC channels, rather than in the aryl substituents. The above experimental and theoretical results of COTh-Ar derivatives showed that even if aromatic substituents were introduced, overpass-shaped TSC channels still played a decisive role in the photophysical properties, which provided valuable guidance for developing derivatives based on COTh structure.

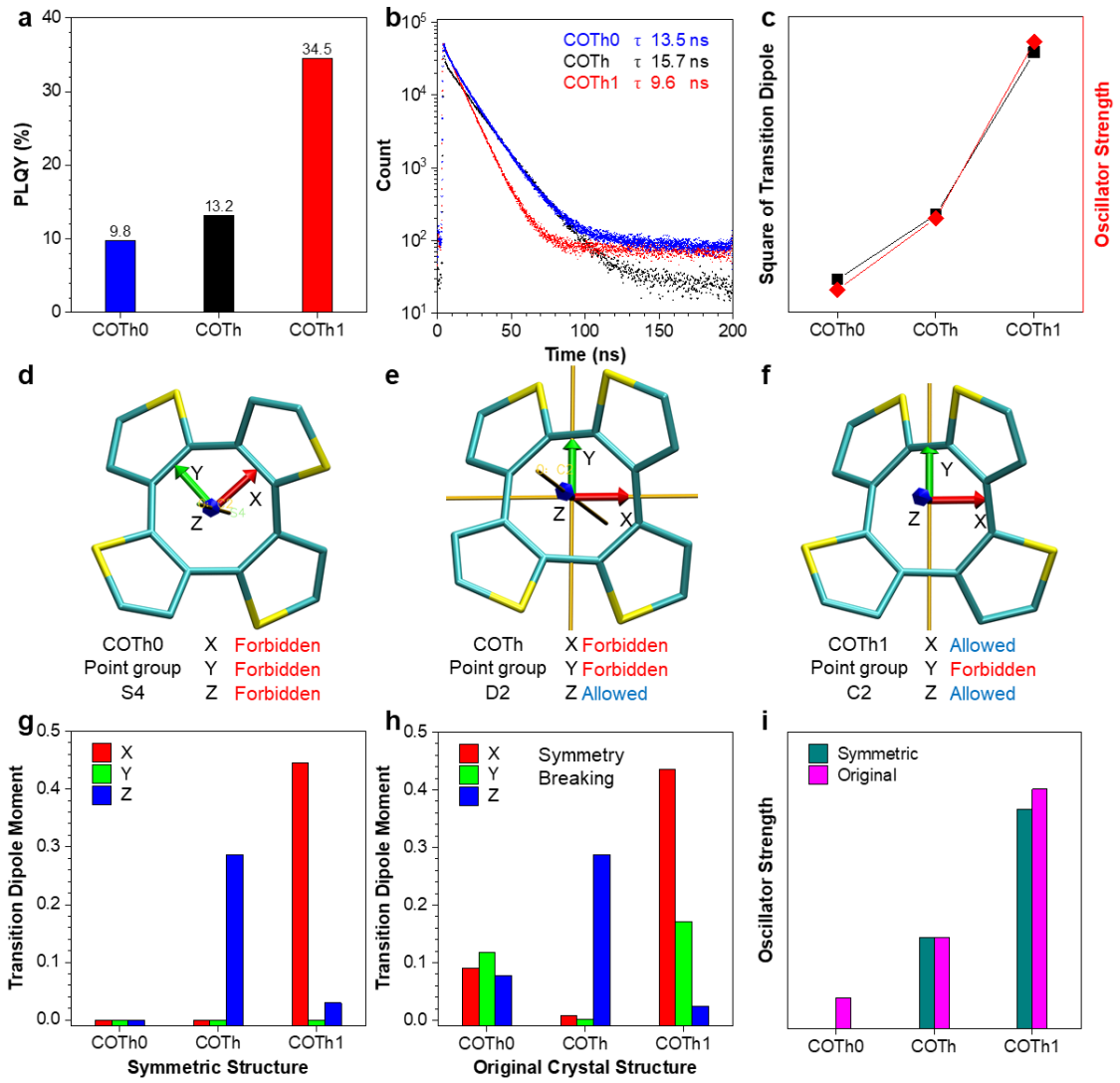

Figure 7.

(a) Quantum yields and (b) fluorescence decay curves of COTh0, COTh, and COTh1 at solid states. (c) Transition dipole moment and oscillator strength of COTh0, COTh, and COTh1. (d-f) Symmetry characteristics (point groups and symmetry axes) and transition allowed directions of the symmetrized crystal structures of (d) COTh0, (e) COTh, and (f) COTh1. (g-h) The transition dipole moments in the XYZ directions in the (g) symmetrized and (h) original crystal structures of COTh0, COTh, and COTh1. (i) Oscillator strengths of COTh0, COTh, and COTh1 in the symmetrized and original crystal structures of COTh0, COTh, and COTh1.

The discovery of 'conjugation anomalous' luminescence in COTh derivatives and the full demonstration of the TSC-dominated luminescence mechanism opened the door to its advanced development. However, the COTh derivatives reported in the literature exhibited low photoluminescence quantum yields (PLQY),[48] which may limit its widespread application. When characterizing COTh, COTh1, and COTh0, it was noticed that their luminescence intensities were quite different, whether in solid powder or aggregated state. As shown in Figure 2a, the AIE factor (α_{AIE}) of COTh1 (α_{AIE} = 38) was significantly higher than that of COTh (α_{AIE} = 7) and COTh2 (α_{AIE} = 6). To confirm the nature of the difference, their fluorescence lifetimes (τ_S) and PLQYs (Φ_F) in the solid state were characterized (Table S5 and Figures 7a-7b). The Φ_F of COTh1 (34.5%) was significantly higher than that of COTh (13.2%) and COTh0 (9.8%). The τ_S of COTh1 (9.6 ns) was shorter than that of COTh (15.7 ns) and COTh0 (13.5 ns). Based on the Φ_F and τ_S, their radiative rates (k_F) and non-radiative rates (k_{Non}) can be calculated. The non-radiative process included the internal conversion (IC) from the S_1 state to the S_0 state and the intersystem crossing (ISC) from the S_1 state to the triplet states (T_n). The non-radiative rates k_{Non} of COTh, COTh1, and COTh0 were not much different: 55.4 × 10^6 s^{-1} for COTh, 68.8 × 10^6 s^{-1} for COTh1, and 66.7 × 10^6 s^{-1} for COTh0. But the radiation rate k_F of COTh1 (35.4 × 10^6 s^{-1}) was much greater than that of COTh (8.3 × 10^6 s^{-1}) and COTh0 (7.4 × 10^6 s^{-1}). These results indicated the high PLQY of COTh1 was mainly due to its high radiation rate.

To understand the origin of radiation rate differences, the transition rates were studied in depth through theoretical calculations (Scheme S1). The experimental radiation rates correspond to the theoretically calculated oscillator strengths. The oscillator strengths consistently correlate with the radiation rates and PLQYs (Figure 7c). According to Equation S1, the oscillator strength is proportional to the product of the energy difference and the squares of the transition dipole moment. The energy differences of COTh, COTh1, and COTh0 were almost equal, so the transition rate difference was dominated by the transition dipole moment. Furthermore, the transition dipole moment is mainly affected by the degree of orbital overlap and symmetry prohibition. The degree of orbital overlap can be characterized by orbital overlap integral.[49, 50] As shown in Figure S15, the orbital overlaps of three isomers were similar, which meant that the apparent transition rate difference might arise from symmetry prohibition in the transition processes.

Based on the crystal structure of COTh, COTh1, and COTh0, after symmetry treatment, the symmetry properties and transition directions of allowed or forbidden were obtained (Figures 7d-7f, Tables S6-S16). The COTh0 crystal structure belonged to the S4 point group and had a S4 symmetry axe in the Z direction. Its transitions in the X, Y, and Z directions were forbidden, so its radiative transition capability was inferior. The COTh crystal structure belonged to the D2 point group and had three C2 symmetry axes in the X, Y, and Z directions. For COTh, transitions in the X and Y directions were forbidden, but transition in the Z direction was allowed, which meant its transition ability was higher than that of COTh0 molecules. The COTh1 crystal structure belonged to the C2 point group and had a C2 symmetry axe in the Y direction. For COTh1, transition in the Y direction was forbidden, while the transitions in the X and Z directions were allowed, giving it a great possibility of transition. Qualitative results based on symmetry analysis preliminarily confirmed that the significant difference in PLQY among the three isomers was derived from the considerable difference in symmetry.

The detailed transition dipole moment values could more intuitively demonstrate the difference in their transition capabilities. The transition dipole moment in each direction based on the symmetrical structure of COTh0, COTh, and COTh1 are shown in Figure 7g. The symmetrical COTh0 molecule had no transition dipole moment in each direction because the symmetry forbidden. The symmetrical COTh molecule had no transition dipole moments in the X and Y directions but had a transition dipole moment of 0.28 in the Z direction. The symmetrical COTh1 molecule had a high transition dipole moment of 0.45 in the X direction and another transition dipole moment of 0.03 in the Z direction. Due to the large number of intermolecular interactions within a crystal, there are always differences between the actual crystal structure and a perfectly symmetrical structure. The transition dipole moments from the original crystal structure without symmetry treatment are shown in Figure 7h. Compared with the transition dipole moments of the symmetrical structure, the dipole moments of the original crystal structures showed apparent differences. In the XYZ directions of COTh0 and the Y direction of COTh1, which were supposed to be transition-forbidden directions, obvious transition dipole moments appeared, indicating that the intermolecular interaction in the crystal made the structure deviated from the symmetrical structure and thereby broke the symmetry forbidden. In fact, the structural

differences between the symmetric structure and the original crystal structure were tiny (Figure S16), indicating that the transition properties of COTh0 and COTh1 might be sensitive to changes in structure and environment. Inspired by this hypothesis, we compared the oscillator strengths of COTh1 molecules in various environments such as gas phase, solvent, and crystal. As shown in Figure S17, in the gas phase, solution, and crystal, the intensity of the transition oscillator increased significantly, proving that the aggregation process enhanced the symmetry breaking. In short, modifying molecular symmetry and aggregation-enhanced symmetry breaking are effective strategies to improve the optical properties of COTh series molecules, which provides crucial guidance for the structural design and application development of high-symmetry organic optical molecules.

Conclusion

This work discovered the 'conjugation anomalous' luminescence behavior of COTh and systematically proved its unique TSC-dominated luminescence mechanism. Due to the particular phase arrangement of the 8-membered COT ring in the COTh molecule, TBC was unfavorable, whereas TSC had a significant impact. COTh exhibited a particular overpass-shaped TSC channel that cut through the molecule and effectively linked the four thiophene rings, expanding the dimensions and forms of non-traditional delocalization. Orbital phase, angle, and spatial action distance were proven critical for TSC effect formation. COTh derivatives, including COTh isomers and aryl-substituted COTh derivatives, were also studied. The results showed that TSC was decisive for the photophysical properties of COTh derivatives.

Furthermore, the TSC analysis tool was developed to provide universal research tools for precise TSC paths, action points, and intensity analysis. In addition, it was proved that symmetry forbidden hindrance was the reason for the generally low PLQY of COTh derivatives. A dual strategy of adjusting structural symmetry and aggregation-enhanced symmetry breaking, which would significantly improve the luminescence performance of COTh derivatives, was proposed. This work comprehensively explains the TSC-dominated luminescence mechanism, provides new models, perspectives, and tools for TSC theory, and is expected to promote the innovation and development of molecules, materials, and applications based on TSC theory.

Acknowledgments

This work was supported by NSFC (52003228 and 52273197), Shenzhen Key Laboratory of Functional Aggregate Materials (ZDSYS20211021111400001), the Science Technology Innovation Commission of Shenzhen Municipality (JCYJ2021324 134613038, KQTD20210811090142053, and GJHZ20210705141810031).

Conflict of interest

The authors declare no competing financial interest.

Data Availability Statement

All data associated with this study are present in the paper or the supplemental information.

Author contributions

Bo Wu, Guoqing Zhang, Zheng Zhao, and Ben Zhong Tang conceived the idea for this work.

Bo Wu prepared the samples, conducted the experiments, collected and analyzed the data, carried out the theoretical calculations, and wrote, revised, and polished the manuscript.

[1] J. Weiss, *Nature* **1943**, *152*, 176.
[2] O. Ostroverkhova, *Chem. Rev.* **2016**, *116*, 13279.
[3] X. Yang, G. I. N. Waterhouse, S. Lu, J. Yu, *Chem. Soc. Rev.* **2023**, *52*, 8005.
[4] W. Xu, M. M. S. Lee, Z. Zhang, H. H. Y. Sung, I. D. Williams, R. T. K. Kwok, J. W. Y. Lam, D. Wang, B. Z. Tang, *Chem. Sci.* **2019**, *10*, 3494.
[5] L. Zhu, L. Tian, S. Jiang, L. Han, Y. Liang, Q. Li, S. Chen, *Chem. Soc. Rev.* **2023**, *52*, 7389.
[6] X. Feng, X. Wang, C. Redshaw, B. Z. Tang, *Chem. Soc. Rev.* **2023**, *52*, 6715.
[7] S. Zeng, X. Liu, Y. S. Kafuti, H. Kim, J. Wang, X. Peng, H. Li, J. Yoon, *Chem. Soc. Rev.* **2023**, *52*, 5607.
[8] C. Wang, Q. Qiao, W. Chi, J. Chen, W. Liu, D. Tan, S. McKechnie, D. Lyu, X. F. Jiang, W. Zhou, N. Xu, Q. Zhang, Z. Xu, X. Liu, *Angew. Chem. Int. Ed.* **2020**, *59*, 10160.
[9] S. Liu, X. Zhou, H. Zhang, H. Ou, J. W. Y. Lam, Y. Liu, L. Shi, D. Ding, B. Z. Tang, *J. Am. Chem. Soc.* **2019**, *141*, 5359.
[10] M. Natali, S. Campagna, F. Scandola, *Chem. Soc. Rev.* **2014**, *43*, 4005.
[11] A. C. Sedgwick, L. Wu, H.-H. Han, S. D. Bull, X.-P. He, T. D. James, J. L. Sessler, B. Z. Tang, H. Tian, J. Yoon, *Chem. Soc. Rev.* **2018**, *47*, 8842.
[12] F. Y. Song, Z. Xu, Q. S. Zhang, Z. Zhao, H. K. Zhang, W. J. Zhao, Z. J. Qiu, C. X. Qi, H. Zhang, H. H. Y. Sung, I. D. Williams, J. W. Y. Lam, Z. J. Zhao, A. J. Qin, D. G. Ma, B. Z. Tang, *Adv. Funct. Mater.* **2018**, *28*, 1800051.
[13] L. Zhang, H.-X. Wang, S. Li, M. Liu, *Chem. Soc. Rev.* **2020**, *49*, 9095.
[14] R. Carr, N. H. Evans, D. Parker, *Chem. Soc. Rev.* **2012**, *41*, 7673.

[15] M. C. Storer, C. A. Hunter, *Chem. Soc. Rev.* **2022**, *51*, 10064.
[16] M. Raynal, P. Ballester, A. Vidal-Ferran, P. W. N. M. van Leeuwen, *Chem. Soc. Rev.* **2014**, *43*, 1660.
[17] J. Xu, S. B. Jo, X. Chen, G. Zhou, M. Zhang, X. Shi, F. Lin, L. Zhu, T. Hao, K. Gao, Y. Zou, X. Su, W. Feng, A. K. Jen, Y. Zhang, F. Liu, *Adv. Mater.* **2022**, *34*, e2108317.
[18] G. R. Desiraju, *J. Am. Chem. Soc.* **2013**, *135*, 9952.
[19] J. Yang, M. M. Fang, Z. Li, *Aggregate* **2020**, *1*, 6.
[20] G. Q. Yin, W. Lu, J. X. Huang, R. Li, D. P. Liu, L. Q. Li, R. H. Zhou, G. F. Huo, T. Chen, *Aggregate* **2023**, *4*, e344.
[21] H. Y. Dong, C. H. Zhang, J. N. Yao, Y. S. Zhao, *Aggregate* **2021**, *2*, e103.
[22] Z. An, C. Zheng, Y. Tao, R. Chen, H. Shi, T. Chen, Z. Wang, H. Li, R. Deng, X. Liu, W. Huang, *Nat. Mater.* **2015**, *14*, 685.
[23] M. Hecht, F. Würthner, *Acc. Chem. Res.* **2021**, *54*, 642.
[24] Z. Zhao, S. Chen, J. W. Y. Lam, C. K. W. Jim, C. Y. K. Chan, Z. Wang, P. Lu, C. Deng, H. S. Kwok, Y. Ma, B. Z. Tang, *J. Phys. Chem. C* **2010**, *114*, 7963.
[25] H. Zhang, Z. Zhao, A. T. Turley, L. Wang, P. R. McGonigal, Y. Tu, Y. Li, Z. Wang, R. T. K. Kwok, J. W. Y. Lam, B. Z. Tang, *Adv. Mater.* **2020**, *32*, e2001457.
[26] J. Guan, R. Wei, A. Prlj, J. Peng, K. H. Lin, J. Liu, H. Han, C. Corminboeuf, D. Zhao, Z. Yu, J. Zheng, *Angew. Chem. Int. Ed.* **2020**, *59*, 14903.
[27] Z. Zhao, H. Zhang, J. W. Y. Lam, B. Z. Tang, *Angew. Chem. Int. Ed.* **2020**, *59*, 9888.
[28] D. Liu, M. Zhang, W. Tian, W. Jiang, Y. Sun, Z. Zhao, B. Z. Tang, *Aggregate* **2022**, *3*, e164.
[29] Z. Zhao, Z. Wang, J. Tavakoli, G. Shan, J. Zhang, C. Peng, Y. Xiong, X. Zhang, T. S. Cheung, Y. Tang, B. Huang, Z. Yu, J. W. Y. Lam, B. Z. Tang, *Aggregate* **2021**, *2*, e36.
[30] S. S. Chen, H. Wang, B. Wu, Q. Li, J. Gong, Y. L. Zhao, Y. Zhao, X. Xiao, J. W. Y. Lam, Z. Zhao, X. D. Luo, B. Z. Tang, *ACS Cent. Sci.* **2023**, *9*, 883.
[31] N. L. Leung, N. Xie, W. Yuan, Y. Liu, Q. Wu, Q. Peng, Q. Miao, J. W. Lam, B. Z. Tang, *Chemistry–A European Journal* **2014**, *20*, 15349.
[32] Q. Zeng, Z. Li, Y. Dong, C. Di, A. Qin, Y. Hong, L. Ji, Z. Zhu, C. K. W. Jim, G. Yu, Q. Li, Z. Li, Y. Liu, J. Qin, B. Z. Tang, *Chem. Commun.* **2007**, 70.
[33] H. K. Zhang, Z. Zhao, P. R. McGonigal, R. Q. Ye, S. J. Liu, J. W. Y. Lam, R. T. K. Kwok, W. Z. Yuan, J. P. Xie, A. L. Rogach, B. Z. Tang, *Mater. Today* **2020**, *32*, 275.
[34] P.-C. Shen, Z.-Y. Zhuang, Z.-J. Zhao, B. Z. Tang, *Chin. Chem. Lett.* **2016**, *27*, 1115.
[35] M. Liu, X. Han, H. Chen, Q. Peng, H. Huang, *Nat. Commun.* **2023**, *14*, 2500.
[36] J. Liu, H. Zhang, L. Hu, J. Wang, J. W. Y. Lam, L. Blancafort, B. Z. Tang, *J. Am. Chem. Soc.* **2022**, *144*, 7901.
[37] J. Zhang, L. Hu, K. Zhang, J. Liu, X. Li, H. Wang, Z. Wang, H. H. Y. Sung, I. D. Williams, Z. Zeng, J. W. Y. Lam, H. Zhang, B. Z. Tang, *J. Am. Chem. Soc.* **2021**, *143*, 9565.
[38] L. Viglianti, N. Xie, H. H. Y. Sung, A. A. Voityuk, N. L. C. Leung, Y. Tu, C. Baldoli, I. D. Williams, R. T. K. Kwok, J. W. Y. Lam, E. Licandro, L. Blancafort, B. Z. Tang, *Angew. Chem. Int. Ed.* **2019**, *59*, 8552.
[39] Z. Zhao, X. Zheng, L. Du, Y. Xiong, W. He, X. Gao, C. Li, Y. Liu, B. Xu, J. Zhang, F. Song, Y. Yu, X. Zhao, Y. Cai, X. He, R. T. K. Kwok, J. W. Y. Lam, X. Huang, D. Lee Phillips, H. Wang, B. Z. Tang, *Nat. Commun.* **2019**, *10*, 2952.
[40] L. Viglianti, N. L. C. Leung, N. Xie, X. Gu, H. H. Y. Sung, Q. Miao, I. D. Williams, E. Licandro, B. Z. Tang, *Chem. Sci.* **2017**, *8*, 2629.
[41] M. Ueda, K. Jorner, Y. M. Sung, T. Mori, Q. Xiao, D. Kim, H. Ottosson, T. Aida, Y. Itoh, *Nat. Commun.* **2017**, *8*, 346.
[42] D. A. Hrovat, W. T. Borden, *J. Am. Chem. Soc.* **1992**, *114*, 5879.
[43] S. C. A. H. Pierrefixe, F. M. Bickelhaupt, *J. Phys. Chem. A* **2008**, *112*, 12816.
[44] P. Politzer, J. S. Murray, J. M. Seminario, *International Journal of Quantum Chemistry* **1994**, *50*, 273.
[45] J. C. Santos, W. Tiznado, R. Contreras, P. Fuentealba, *J. Chem. Phys.* **2004**, *120*, 1670.
[46] T. Lu, F. Chen, *Acta Phys-Chim. Sin.* **2011**, *27*, 2786.
[47] R. F. W. Bader, *Chem. Rev.* **1991**, *91*, 893.
[48] Y. J. Yang, Y. R. Gu, Z. Y. Ma, Y. L. Zhang, W. Xu, L. Xu, K. Wang, B. Zou, H. Wang, *Dyes Pigments* **2021**, *184*.
[49] T. Lu, F. Chen, *J. Comput. Chem.* **2012**, *33*, 580.
[50] P. Ramesh, M. Lydia Caroline, S. Muthu, B. Narayana, M. Raja, S. Aayisha, *J. Mol. Struct.* **2020**, *1200*,

127123.